1-16-2020

The Al-induced proteomes of epidermal and outer cortical cells in root apex of cherry tomato 'LA 2710'

Shaolan Yang
Tennessee State University

Hui Li
Tennessee State University

Sarabjit Bhatti
Tennessee State University

Suping Zhou
Tennessee State University

Yong Yang
Cornell University

See next page for additional authors

Recommended Citation

Shaolan Yang, Hui Li, Sarabjit Bhatti, Suping Zhou, Yong Yang, Tara Fish, Theodore W. Thannhauser, "The Al-induced proteomes of epidermal and outer cortical cells in root apex of cherry tomato 'LA 2710'", Journal of Proteomics, Volume 211, 2020, 103560, ISSN 1874-3919, https://doi.org/10.1016/j.jprot.2019.103560.

The Al-induced proteomes of epidermal and outer cortical cells in root apex of cherry tomato 'LA 2710'

Shaolan Yang[a,b], Hui Li[a], Sarabjit Bhatti[a], Suping Zhou[a]*, Yong Yang[c], Tara Fish[c] and Theodore W. Thannhauser [c]*

[a]*Department of Agricultural and Environmental Sciences, College of Agriculture, Tennessee State University, 3500 John Merritt Blvd, Nashville, TN 37209, USA*

[b]*College of Horticulture, Qingdao Agricultural University, Qingdao, Shandong, P.R. China. 266109, China*

[c]*R.W. Holley Center for Agriculture and Health, USDA-ARS, Cornell University, Ithaca, NY 14853, USA*

*Correspondence: zsuping@tnstate.edu (S.Z.); tt34@cornell.edu (T.W.T.); Tel.: +1-615-963-2465 (S.Z.); +1-607-255-8808 (T.W.T.)

ABSTRACT

This paper reports a laser capture microdissection-tandem mass tag-quantitative proteomics analysis of Al-sensitive cells in root tips. Cherry tomato (*Solanum lycopersicum* var. *cerasiforme* 'LA2710') seedlings were treated under 15 µM Al^{3+} activity for 13 d. Root-tip longitudinal fresh frozen tissue sections of 10 µm thickness were prepared. The Al-sensitive root zone and cells were determined using histochemical analysis of root-tips and micro-sections. A procedure for collecting the Al-sensitive cells using laser capture microdissection-protein extraction-tandem mass tag-proteomics analysis was developed. Proteomics analysis of 18 µg protein/sample with three biological replicates per treatment condition identified 3879 quantifiable proteins each associated with two or more unique peptides. Quantified proteins constituted a broad range of Kyoto Encyclopedia of Genes and Genomes pathways when searched in the annotated tomato genome. Differentially expressed proteins between the Al-treated and non-Al treated control conditions were identified, including 128 Al-up-regulated and 32 Al-down-regulated proteins. Analysis of functional pathways and protein-protein interaction networks showed that the Al-down-regulated proteins are involved in transcription and translation, and the Al-up-regulated

proteins are associated with antioxidant and detoxification and protein quality control processes. The proteomics data are available via ProteomeXchange with identifier PXD010459 under project title 'LCM-quantitative proteomics analysis of Al-sensitive tomato root cells'.

Significance

This paper presents an efficient laser capture microdissection-tandem mass tag-quantitative proteomics analysis platform for the analysis of Al sensitive root cells. The analytical procedure has a broad application for proteomics analysis of spatially separated cells from complex tissues. This study has provided a comprehensive proteomics dataset expressed in the epidermal and outer-cortical cells at root-tip transition zone of Al-treated tomato seedlings. The proteomes from the Al-sensitive root cells are valuable resources for understanding and improving Al tolerance in plants.

Keywords: laser capture microdissection-tandem mass tag-proteomics, single cell type root-tip proteomics, tomato, Al stress, protein functional classification, protein-protein interaction network

1. Introduction

In acidic soil (i.e., pH < 5.0) Al^{3+} ions are released from soil clay into soil solutions. Upon uptake into roots, these positively charged Al^{3+} ions bind strongly to the negatively charged cell walls. This type of interaction results in rapid production of reactive oxygen species (ROS), significant rigidity and loss of elasticity of cell walls, particularly of the epidermis and outer cortical cells [1]. Ruptures of these cell layers damage root tips and result in stunted and deformed roots.

There are no transporters or channel proteins in cell membranes that would selectively facilitate the passage of Al^{3+} ions into the symplast spaces; Al^{3+} ions are simply stronger competitors for binding to the ion transporters in the plasma membrane [2]. More importantly, Al^{3+} ions have a smaller ionic radius (0.54 Å), and larger surface charge compared to Ca^{2+} (0.99 Å) and Mg^{2+} (0.86 Å), thus they bind more readily to the transporters of these essential mineral elements. The obstruction of these ion channels leads to a deficiency of these essential elements

in plants. The Al-induced inhibitory effect on plant root growth was first reported over a century ago [3] and a majority of plants species are susceptible to the excess Al concentrations in acid soil [4, 5].

The root tip is the major site for the perception of Al^{3+} ions [5-7]. By convention we identify four distinct regions along the longitudinal axis of the primary roots: the apical meristematic zone (AMZ), transition zone (TZ), elongation zone (EZ) and maturation zone (MZ) [8-10]. The root transition zone (TZ) is located between AMZ and the basal EZ. The TZ has a key role in balancing cell division to cell differentiation, to sustain coherent root growth, and thus the length of the root tips. A great number of studies have shown that TZ represents the most sensitive root zone to Al toxicity and the induced cellular damages [9, 11, 12-14]. More precisely, the outermost epidermal cells and the outer cortical layer which provide feeder cells for the replacement of epidermis are the main target of Al^{3+} ions in root apices [12-15]. Exudation of organic acids to immobilize Al^{3+} in rhizosphere is a major mechanism for Al tolerance. Al-resistant plants have evolved effective strategies that precisely localize root citrate exudation to the TZ [16]. Furthermore, application of boron (B) was found to promote root surface alkalization in TZ, to thus reduce Al accumulation in the apoplastic space and the internalization of the toxic ions in the TZ cells [17]. More studies also showed that Al^{3+} ions affect concentration gradient of hormones including auxins, cytokinins, ethylene, jasmonic acid (JA), and gibberellins (GA) in the TZ locales, which can in turn disturb biological processes such as cell division, growth, cell polarity, cell differentiation, and root growth [18,19].

Despite accumulating evidence for the importance of TZ cells in Al tolerance, the relevant molecular understanding of the Al-induced proteomics changes is still very limited. This is partially caused by the difficulty in sample collection of these TZ cells. Laser capture microdissection (LCM) is a procedure to isolate specific cell types or defined regions from a whole tissue sections under microscope. The analysis of the LCM collected cells can provide an understanding of functions of each individual member in a complex, multicellular processes [20-22]. The LCM-enabled molecular analysis technology reported here would be an ideal analytical approach for the dissection of the molecular mechanisms underlying Al toxicity in the TZ.

Previously, we have reported LCM capture of epidermal/outer cortical cells from cross sections of Al-treated tomato roots [23]. In our experience, the LCM proteomics analysis of the Al-sensitive TZ cells is fraught with a host of technical challenges, not the least of which is isolating the large number of cells required, extraction of high quality proteins from extremely small amount of plant tissue, and quantitative identification of a larger number of proteins from a small amount of sample. In this study, we have developed a LCM-TMT-proteomics platform for studying Al sensitive cells in roots.

Cherry tomato 'LA2710' to be analyzed in this study was first discovered growing in tropical soils with low pH and high Al content in Brazil; it was thus hypothesized to be an Al tolerant variety [24]. In our own variety trial for Al tolerance, 'LA2710' was also found to be more Al-tolerant than 'Micro-Tom' (Zhou SP, unpublished data). Therefore, the proteomes identified in this study are relevant to Al tolerance mechanisms.

2. Materials and methods

2.1 Plant material preparation and Al treatments

Tomato seed stocks were obtained from Tomato Genetic Resource Center, UC Davis, USA [24]. Seeds were propagated on self-pollinated plants grown in a greenhouse on Agricultural Research Station, Tennessee State University, Nashville, TN, USA. In this experiment, seeds were disinfected by soaking in 0.5% (w/v) NaOCl for 15 min followed by three rinses in sterilized H_2O. Seeds were soaked for 24 h in either –Al (non-Al-treated control) or +Al (100 µM $AlK(SO_4)_2 \cdot 12H_2O$ providing 15 µM ion activity, Al-treated) Magnavaca's nutrient solution, pH 4.5 [25]. Rockwool seed cubes were washed three times in either Al-treated or non-Al-treated control solution in hydroponic tanks. Approximately 800 seeds were planted in each tank, and three tanks each for Al-treated or non-Al-treated control conditions were set-up. Treatment solutions were refreshed every day. The treatment experiments were terminated after 13 days when cotyledons expanded but no true leaves emerged. Based on our experience, once when true leaves expand, plant roots start branching and growing into the fiber in the seed cube, which makes it very difficult to harvest intact root tips. For tissue collection, radicles were carefully removed from seed cubes. Tissues from each tank were pooled together into one

biological replicate, and three replicates each for Al-treated and non-Al-treated conditions were collected. The treatment experiment was conducted in a glass greenhouse with temperature set at 25/22 °C (14/10 h; day/night) with no supplemental light.

2.2 Preparation of microdissection slides of root-tips

Immediately upon detaching from the plants, root tips were placed in a pre-chilled fixative solution (75% ethanol + 25% acetic acid). Root-tips were infiltrated under vacuum for 15 min each in sequential order as: fixative solution, twice in phosphate buffered saline (PBS), pH 8.0, 10% sucrose, the Halt Protease Inhibitor Cocktail (1:100, v/v) (Fisher Scientific, MA USA), and the same buffer twice except with 20% sucrose. Root tips were imbedded in optimum cutting temperature (OCT) compound (Fisher Scientific). Roots were cut into 10 µm thickness longitudinal sections using a LEICA CM 1950 cryostat (Leica, Germany), and then transferred to a pre-coated adhesive slide using the CryoJane Tape-Transfer System. Slides were stored at -20 °C when used for picking cells immedicably, or they were kept at -80 °C for long-term storage.

2.3 Microscopic analysis to determine the Al-sensitive root zones and cell layers in root-tips.

For whole root-tip staining, seedling were removed from the Al-treated and non-Al-treated control solutions followed by three washes in de-ionized water each for 10 min. To determine binding of Al to roots, roots were exposed for 10 min to a solution of 0.2% hematoxylin and 0.02% potassium iodide (w/v) at 25 °C under continuous shaking [26,27]. After incubation, root-tips stained with hematoxylin were visualized under bright light field under a SZX16 Olympus stereomicroscope (Olympus America Inc., PA, USA). The accumulation of reactive oxygen species (ROS) was detected using a fluorescent dye of 2,7-dichlorofluorescin diacetate (DCFDA) following the method described earlier [28]. After two rinses in 250 mM Tris-HCl buffer (pH8.0), root-tips were submerged in 25 µM DCFDA (Molecular Probes, OR, USA) in 250 mM Tris-HCl (pH8.0) at 37 °C for 30 min. After labeling, the DCFDA fluorescence was visualized and imaged with a BP450-490 excitation filter under a ZEISS M2 Apotome.2 Imager (ZEISS, Oberkochen, Germany). To determine the Al-sensitive cells, the root-tip microsection slides were stained in hematoxylin solution for 1 min following

the same procedure as described above. After three rinses in de-ionized water, tissue sections were visualized and imaged using the same ZEISS Imager.

2.4 Laser capture microdissection collection of Al-sensitive cells

After two washes in 75-95% ethanol each for 2 min, slides were rinsed in absolute ethanol. TZ cells were captured by cutting the region of interest into the capture caps using the PALM MicroBeam LCM with UV laser system (ZEISS). Based on the above-described microscopic analysis, approximately 8-10 cells per layer and 16-20 cells from the epidermal and outer cortical layers on each side of a section were captured, and two cuts (elements) were made on each section. For each biological replicate sample, approximately 5000 elements from 2500-sections containing 80,000-100,000 cells were collected. Based on our observation under the LCM microscope, each root-tip produced 4-5 good sections, yielding 8-10 LCM elements (with clearly defined structures), so each biological sample should be collected from approximately 500 root-tips. Three replicates each were captured for Al-treated and non-Al treated control groups.

2.5 Protein extraction from LCM-captured samples and labeling peptide with tandem mass tags

Proteins were extracted following a single step protein extraction protocol developed for LCM captured samples with minor modifications [29]. Briefly, the LCM captured cells were transferred into a 50 µl Pressure Cycling Technology (PCT) tube (Pressure Biosciences Inc, PBI, NY, USA). Protein was extracted in 35 µl PCT buffer composed of 20 mM 4-(2-hydroxyethyl)-1-piperazineethanesulfonic acid (HEPES), pH 8.0, 4 M urea, 2% sodium dodecyl sulfate (SDS), 2 mM ethylenediaminetetraacetic acid (EDTA) in a Barocycler (2320 EXT; PBI) running at 45 kPsi pressure for 60 cycles at 25 °C. After completion of the cycles, protein extracts were transferred from the PCT tube into a 1.5 ml Eppendorf tube and centrifuged at 16,873*g* for 10 min at 4 °C. Protein concentration in the supernatant was measured using Qubit Protein Assay kit (Fisher Scientific), on a Qubit 3.0 Fluorometer (Life Technologies Corporation, NY, USA).

Eighteen µg proteins were taken from each sample. After reduction in Tris (2-carboxyethyl) phosphine (TCEP), cysteines were blocked with methyl methanethiosulfonate (MMTS). Samples were processed using the S-TRAP Micro column (PROTIFI, NY, USA)

following the manufacturer's instructions to remove SDS and urea. On-column trypsin digestion was carried out using the sequencing grade modified trypsin (Promega, WI, USA) at 35 °C for 16 h. Tryptic peptides were eluted by centrifugation (4000*g* for 30 s) in 40 µL 50 mM triethylammonium bicarbonate (TEAB) buffer, 40 µL 0.2% formic acid (FA), and finally 40 µL 50% acetonitrile (ACN) in water and 0.2% FA, with centrifugation between each wash. Eluted fractions were combined and dried under reduced pressure. After reconstitution in 50 mM TEAB, peptides were labeled with TMT tags (126, 127, 128 for the three Al-treated replicates, and 129,130, 131 for the three non-treated control replicates), using the TMT six-plex label reagent set (ThermoFisher Scientific, CA, USA). Labeled peptides were pooled; SDS salts and unbound tags were removed using the Oasis MCX 1 ml 30 mg Extraction Cartridges (Waters, MA, USA). Peptides were eluted twice in 75% ACN/10% NH_4OH and dried-down under vacuum.

2.6 High pH reverse phase (hpRP) fractionation and nano liquid chromatography and mass spectrometry analysis (LC-MS/MS)

The hpRP chromatography was carried out using a Dionex UltiMate 3000 HPLC system with UV detection (ThermoFisher Scientific) as reported previously [30]. Specifically, the TMT 6-plex tagged tryptic peptides were reconstituted in buffer A (20 mM ammonium formate, pH 9.5 in water), and loaded onto an XTerra MS C18 column (3.5 µm, 2.1 x 150 mm) from Waters (Milford, MA, USA). The peptides were eluted using a gradient of 10-45% buffer B (80% ACN/20% 20 mM NH_4FA) in 30 min at a flow rate 200 µL/min. Forty-eight fractions were collected at 1 min intervals and pooled into a total of 6 fractions based on the UV absorbance at 214 nm and with a multiple fraction concatenation strategy. All of the fractions were dried and reconstituted in 40 µL of 2% ACN/0.5% FA for nanoLC-MS/MS analysis.

NanoLC-MS/MS analysis was carried out using an Orbitrap Fusion (ThermoFisher Scientific) mass spectrometer equipped with a nano ion source using higher energy collision dissociation (HCD) similar to previous reports [30]. The Orbitrap was coupled with an UltiMate3000 RSLCnano (Dionex; ThermoFisher Scientific). Each reconstituted fraction (8 µL) was injected onto a PepMap C-18 RP nano trap column (3 µm, 75 µm × 20 mm, Dionex) at 20 µL/min flow rate for on-line desalting. They were eluted from the trap column and separated

using a PepMap C-18 RP column (3 µm, 75µm x 15cm), by eluting with a 120 min gradient of 5% to 38% ACN in 0.1% FA at 300 nL/min. The chromatographic gradient was followed by a 7-min ramp to 95% ACN/0.1% FA and a 7-min hold at 95% ACN/0.1% FA. The column was then re-equilibrated with 2% ACN/0.1% FA for 20 min prior to the next run. The Orbitrap Fusion was operated in positive ion mode with the spray voltage set at 1.6 kV and the source temperature at 275 °C. The FT, IT and quadrupole mass analyzers were calibrated externally. An internal calibration was performed using the background polysiloxane ion signal at *m/z* 445.120025 as the calibrant. The instrument was operated in data-dependent acquisition (DDA) mode using the FT mass analyzer to conduct survey MS scans for selecting precursor ions, followed by 3 s, top speed, data-dependent HCD-MS/MS scans of precursor ions with between 2-7 positive charges and threshold ion counts of > 10,000. The normalized collision energy was 37.5%. MS survey scans were conducted at a resolving power of 120,000 (fwhm) at m/z 200, for the mass range of m/z 400-1600 with AGC and Max IT settings of 3e5 and 50 ms, respectively. MS/MS scans were conducted at a resolution of 50,000 (fwhm) for the mass range m/z 105-2000 with AGC and Max IT settings of 1e5 and 120 ms. The Q isolation window was set at +/- 1.6 Da. Dynamic exclusion duration was set at 60 s with a repeat count of 1, a 50 s repeat duration and a ± 10 ppm exclusion mass width. All data was acquired under Xcalibur 3.0 operation software and Orbitrap Fusion Tune 2.0 (ThermoFisher Scientific).

2.7 Processing of the mass spectrometry data

All MS and MS/MS raw spectra from each set of TMT 6-plex experiments were processed and searched using Sequest HT software within Proteome Discoverer 2.2 (PD 2.2, ThermoFisher Scientific) against tomato protein database version ITAG3.20. The search settings used for protein identification in PD 2.2 were: trypsin digestion allowing two missed cleavages, fixed modifications included carbamidomethyl of cysteine and TMT modifications on lysine ε and peptide N-terminal amines. The variable modifications included methionine oxidation and deamidation of asparagine and glutamine residues. The peptide mass tolerance and fragment mass tolerance values were 10 ppm and 50 mDa, respectively.

Identified peptides were filtered for a maximum 0.05% false discovery rate (FDR) using the Percolator algorithm in PD 2.2. Peptide confidence was set to high. The TMT 6-plex

quantification method within PD 2.2 was used to calculate the reporter ratios. Only peptide spectra containing all reporter ions were designated as "quantifiable spectra" and used for peptide/protein quantitation.

2.8 The quantified proteomes and statistical analysis

In the quantitative proteins analysis, only proteins quantified with two or more unique peptides were included. The protein abundance ratio (treated/non-treated control; T/C)) in PD 2.2 report was log2 transformed, and the Log_2Fold (T/C) values of all the quantified proteins were fitted to a normal distribution to obtain the standard deviation (SD) using SAS (v9.0) software (SAS Inc., NC, USA) [31]. The differentially expressed proteins (DEPs) were selected by passing the following criteria: Log2Fold > 2SD or < -2SD, $p \leq 0.05$ using a *post hoc* Tukey HSD test in PD 2.2, and quantified with two or more unique peptides.

2.9 Functional analysis

To analyze the involvement in cellular processes, the quantified proteins were analyzed for functional classification in two different categories of Gene Ontology (GO): molecular functions, and cellular components, using the Plant MetGenMAP system [32]. The quantified proteins were searched in the STRING (Search Tool for the Retrieval of Interacting Genes) software (v11) [33] to generate a list of matching proteins from *Solanum lycopersicum*. The Kyoto Encyclopedia of Genes and Genomes (KEGG) pathways enriched with the listed proteins were identified using the established criteria of adjusted *p-value* < 0.05.

2.10 Network analysis

Network analysis was performed submitting DEPs to the STRING database [33]. Proteins were represented with nodes and interactions with continuous lines to represent direct interactions (physical), while indirect ones (functional) were represented with interrupted lines. Cluster networks were created using the MCL inflation parameter (MCL = 3) on the STRING website [34]. The protein-protein association network containing quantitative changes of the proteins was visualized in Cytoscape [35].

252 *2.11 Additional Information*

253 Mass spectrometric raw data were deposited to the ProteomeXchange Consortium via
254 the PRIDE partner repository with the dataset identifier PXD010459 under project title "LCM-
255 quantitative proteomics analysis of Al-sensitive tomato root cells"
256 ((https://www.ebi.ac.uk/pride/archive/projects/PXD010459).

257 **3. Results and discussion**

258 *3.1 Determination of Al sensitive cells of root tips for the laser capture microdissection*
259 *procedure*

260 One of the most striking properties for Al-stress is the differential responses
261 (sensitivity) of root cells along the longitudinal and transverse directions in root apex. Using
262 the LCM procedure to isolate cells of interest makes the down-stream analysis better targeted
263 to the relevant biological activities. To locate, precisely, the Al-sensitive zone, we first
264 conducted a histochemical staining analysis using whole roots and the frozen root-tip sections
265 (Fig. 1). In the DCFDA staining analysis, the Al-treated root tips showed a stronger
266 fluorescence which indicates higher ROS accumulation compared to the non-Al-treated roots
267 (A). The Al-treated root-tips stained dark red with hematoxylin showing Al accumulation
268 whereas the non-Al-treated root-tips stained much lighter (B). Results from these analysis on
269 whole root-tips concur with the reported accumulation of Al^{3+} in root apex and activation of
270 oxidative burst when plant roots are exposed to excess Al [36, 37].

271 When the slides were stained with hematoxylin, those prepared using the non-Al-treated
272 root-tips showed a lighter and consistent stain across the root section (C). On the hematoxylin-
273 stained sections from Al-treated root-tips, the epidermal and outer cortical layers stained darker
274 compared to the apical meristem region covered under the root-cap and inner tissues. These
275 results demonstrated that the epidermal and outer-cortical layers contained the most Al-sensitive
276 cells. Thus the basal ~100 µm region from the peripheral cells of root cap up to the cell
277 elongation zone was defined as the TZ in this study, and 8-10 cells were counted on the
278 epidermal and cortical layers each (D).

3.2 Performance of the laser capture microdissection-quantitative proteomics analysis

The epidermal and outer cortical layer cells in the TZ region were harvested using LCM (Fig. 2). For each biological replicate samples, 80,000-100,000 cells comprising the epidermal and outer-cortical layers of cells were captured from approximately 2500 sections of root-tips. Three replicates each were captured for Al-treated and non-Al treated control groups. Using the PCT protein extraction method, each LCM samples yielded 20-25 µg protein. Furthermore, the whole protein extraction procedure was completed in the same tube and within one hour. This has demonstrated a significant improvement in the protein extraction procedure compared to the method used in our previous study which took two days involving manual tissue grinding, followed by protein extraction using dense SDS method, and protein precipitation [23]. The protein yield is much higher than a reported study on root pericycle cells of maize (*Zea mays*) where 30 µg of proteins was extracted from 200, 000 cells [38].

Then we used 18 µg protein for the on-column tryptic digestion. Nano-LC MS/MS analysis identified 5780 proteins. Among proteins containing quantified peptides (reporter ions) across all the six biological samples, 3879 proteins are associated with 2 and more unique peptides, and 856 proteins has one unique peptide (Supplementary Table S1). The distribution of the number of proteins decreased with increasing number of peptides assigned to a protein. A majority (82%) of the quantified proteins contained at least two quantified unique peptides and these proteins were used in comparative protein quantification analysis to identify Al-induced proteome changes (Fig. 2).

The coverage of the quantified proteomes against the annotated tomato genome was evaluated using KEGG pathway analysis (Fig. 3, supplementary Table S2). The 3879 quantified proteins constituted two major categories: Metabolism, and Processing of Genetic Information. The KEGG Metabolism category is represented with pathways for the biosynthesis, degradation, metabolisms of carbohydrates, amino acids, glycan, lipids, cofactors and vitamins, terpenoids, polyketides and nucleotides, and energy regeneration. When the number of the identified proteins was compared to those in the annotated tomato genome database, the percentage of coverage was 63% (147 /232; identified/background proteins) for biosynthesis of amino acids (sly01230), 91% in lysine biosynthesis (sly00300), 60% (79/132) for glycolysis /

gluconeogenesis (sly00010), 70% (38/154) for citrate cycle (TCA cycle) (sly00020), and above 50% for a larger number of KEGG pathways (Fig. 3A).

In the category of Processing of Genetic Information, quantified proteins constituted pathways of DNA replication (base excision repair, mismatch repair and nucleotide excision repair), transcription pathway (comprises of basal transcription factors, RNA polymerase, and spliceosome), protein translation (aminoacyl-tRNA biosynthesis, mRNA surveillance pathway, ribosome, ribosome biogenesis in eukaryotes, and RNA transport), protein folding, sorting and degradation (proteasome, ubiquitin mediated proteolysis, protein processing in endoplasmic reticulum, protein export, SNARE interactions in vesicular transport, and RNA degradation), (Fig. 3B). In this category, the proteasome (sly03050) pathway has the highest coverage of 78% (38/49). Pathways enriched with more than 90 proteins include spliceosome (102), ribosome (117) and protein processing in ER (96). These results show that the quantified proteins are involved in all the major cellular processes in the annotated tomato genome. These demonstrated the efficiency of the LCM-TMT-proteomics workflow in the quantitative proteomics analysis of tomato root TZ cells. Thus the quantified proteins were used for the identification of differentially expressed proteins (DEPs) induced under Al-treated conditions as described below.

3.3. Identification of Al-induced differentially expressed proteins (DEPs)

The Log2Fold (T/C) value of the quantified proteins were subjected to Goodness-of-Fit tests for normal distribution (Supplementary Fig. S1). The dataset passed the Kolmogorov-Smirnov test ($p < 0.01$), the Cramer-von Moses and Anderson-Darling tests ($p < 0.005$). The standard deviation (SD) was 0.337, and proteins with Log2Fold values greater than 2SD should give 95% confidence in abundance differences from Al-treated to non-treated conditions [31]. Thus, differentially expressed proteins (DEPs) were selected passing the following three criteria: Log2Fold (T/C) ≥ 0.67 or ≤ -0.67, $p \leq 0.05$ in the *p-value* of protein abundance ratio in PD 2.2 report, and containing two or more unique peptides. Of the 3879 quantified proteins, 160 DEPs (accounting for 3.3% of quantified proteins) were identified comprising 128 Al-up-regulated and 32 Al-down-regulated proteins (supplementary Table S3).

3.4. Functional classification of Al-induced differentially expressed proteins (DEPs)

The DEPs were analyzed for functional pathways using Plant MetGenMap classification system (Fig. 4, Supplementary Table S4). The cell component classification analysis divided the identified proteins into 22 categories for the Al-up-regulated DEPs and 18 categories for the Al-down-regulated DEPs (Fig. 4A). While most of the GOs were enriched with a large number of Al-up-regulated proteins, cell nucleolus and ribosomes contained a larger number of Al-down-regulated DEPs than the Al-up-regulated DEPs. In the classification of molecular functions, the Al-up-regulated proteins were enriched into 22 categories and the Al-down-regulated proteins into 16 categories. The Al-up-regulated proteins were clustered into the following groups: protein binding, catalytic, hydrolases, transferase activity, and enzyme regulator activity functional categories. Functional groups associated with RNA binding, DNA binding, translation factor activities contained a greater number of Al-down-regulated than Al-up-regulated proteins (Fig. 4B).

The identified DEPs were classified into 10 Pfam families (Fig.5, supplementary Table S5). Seven Pfam families contain proteins from the Al-up-regulated protein group, which include peroxidase, glutathione-S-transferase (GST), pathogenesis-related proteins, phosphate-induced protein 1, PLAT/LH2 domain, trypsin and protease inhibitor and annexin. Exposure to excess levels of Al^{3+} induces generation of oxidative stress in roots [36, 37]. In this study, DCFCA staining also provided experimental evidence of ROS accumulation in Al-treated tomato root tips as shown in Fig. 1A. The enrichment of peroxidase and GST families concurs with their function as major antioxidant and detoxification systems against oxidative stress in cells.

In contrast, the ribosomal L28e protein family was constituted with proteins from the Al-down-regulated DEPs group. Ribosomal protein L28e forms part of the 60S ribosomal subunit, which is involved in translation and ribosome biogenesis. The substantial reduction of these ribosomal proteins was reported to affect protein translation, cell cycle and stress responses [39-41]. Topf et al. [42] using a yeast system, demonstrated that increased levels of intracellular ROS caused by dysfunctional mitochondria serve as a signal to attenuate global protein synthesis. These results also concur with our previous proteomics analysis which have consistently identified stress-repressed DEPs in protein translation machinery in Al, or salt-treated tomatoes [31, 40, 41]. The Al-induced changes in these proteins are in support of the important role in reprogramming of ribosome proteins and the translation machinery to activate stress response

[43-46,]. Three proteins (Solyc04g074400.1.1, Solyc04g074450.1.1, Solyc04g074470.1.1, 1.93-3.31─ fold) were clustered in the family of phosphate-induced protein 1 (*PHI-1*) (PF04674). The *PHI-1* and homologous genes were shown to respond to stress hormones such as abscisic acid (ABA), brassinosteroid (BR) and ethylene, and thus enhancing tolerance to several types of stress [47-48]. The increases of these PHI proteins in the Al treated TZ cells reveal that these proteins (and the encoding genes) may also have a role in Al-stress responses.

The Al-induced DEPs were classified into six KEGG pathways, which include the phenylpropanoid biosynthesis (sly00940), glutathione metabolism (sly00480), metabolic pathways (sly01100), biosynthesis of secondary metabolites (sly01110), glyoxylate and dicarboxylate metabolism (sly00630) and linoleic acid metabolism (sly00591) (Table 1). The phenylpropanoid biosynthesis (KEGG) pathway is enriched with 12 peroxidases, hydroxycinnamoyl CoA quinate transferase (HQT), caffeoyl-CoA 3-O-methyltransferase (CCoA*O*MT), and beta-glucosidase, and all of these proteins were up-regulated in Al-treated roots. The phenylpropanoid pathway is the source of a wide variety of secondary metabolites such as flavonoids, anthocyanins, polyphenols, and lignin monomers, and this pathway is activated as a major mechanism to enhance plant tolerance to several stress factors [49-51]. In grape, the CCoAOMTs was found to act on anthocyanins to induce anthocyanin methylation and thus to increase its stability under drought stress [52]. The TZ cells undergo a transition from primarily mitotic activity to a gradual increase in elongation growth; they are highly sensitive to environmental disturbance [8, 11]. Thus the phenylpropanoid pathway may function as a highly sensitive mechanism to modulate the stress responses.

Cell walls in the TZ are marked by the occurrence of pectin, which are the major binding site of Al^{3+}. Binding of Al to the pectic matrix are closely positively correlated to Al-induced callose deposition at plasmodesmata causing blockage of symplastic transport and communication in higher plants [53]. Callose accumulation was taken as an early marker for Al toxicity [54]. Callose is degraded under the action of glucan endo-1, 3-β-D-glucosidases. In the Al-treated roots, a significant increase in the beta-glucosidase (Solyc12g014420.1.1, 2.34-fold) may have a function in degrading callose and thus reducing the impacts from Al toxicity in the epidermal and outer cortical TZ cells.

Glutathione-S-transferase (GST) is a major system for ROS scavenging and the alleviation of oxidative damage and cellular detoxification under Al stress [55]. The induction of eight GSTs further validated the function of these proteins as major proteins in Al-stress response. The metabolic pathways including secondary metabolites are involved in biosynthesis and degradation of essential amino acids, and post-translational modifications of cell wall protein such as hydroxyproline-rich glycoproteins (HPRGs) which is catalyzed by prolyl 4-hydroxylase [56].

The glyoxylate and dicarboxylate metabolism KEGG pathway contains three proteins: formic acid (formate) dehydrogenase (FDH), catalase isoenzyme 1, and a 4-coumarate-CoA ligase-protein. Formic acid can suppress enzymatic activity in mitochondrial respiration, it accumulated rapidly in rice bean root apices upon Al treatment [57]. Formate dehydrogenase catalyzes the oxidation of formate into CO_2, overexpression of FDH led to a decrease of formate accumulation and enhanced Al and H + stress tolerance in transgenic tobacco plants [58, 59]. Taken together, an increase in FDH abundance may serve a role in the detoxification mechanisms in the Al-treated TZ cells.

3.5 Network analysis of the differentially expressed proteins (DEPs)

Analyzing only the DEPs using STRING v11.0 software after applying MCL clustering, the expected number of edges was 89, where current set of proteins showed 120 (Supplementary Fig. S2, Table S6). This means that the network has significantly more interactions than it would be expected for a random set of proteins of similar size [34]. The underlying molecular regulation may involve function activation or repression of appropriate genes encoding for these proteins, especially those with the highest number of protein-protein interactions and the interconnected clusters.

The 160 proteins formed 20 clusters at the minimum required interaction score of 0.400 (medium confidence). The protein-protein association network was visualized integrating with Log_2Fold values of the identified proteins using Cytoscape software (Fig. 6, Supplementary Table S7). In the network, 11 clusters (cluster 1, 2, 3, 5, 8, 9, 13, 14, 15, 18, 20) are inter-connected. Cluster 1 comprises of seven ribosomal proteins (101244604,

101247801,101251592,101253271, 101266399, Solyc06g062500.2.1, Solyc10g084310.1.1), the eukaryotic peptide chain release factor 1 (Solyc12g010520.1.1), and two elongation factor 1-alpha proteins (101264700, Solyc06g009970.2.1), all involved in protein translation. The cluster 1 is associated with cluster 8 (101247093 for proteasome and 101253687 for ubiquitin) where both proteins increased in abundance under Al-treated condition. These two clusters represent a combination of a decreased protein biosynthesis and an increased proteome quality control under the Al-treated condition.

Cluster 2 is comprised of DNA-directed RNA polymerase subunit A (RPE1), DNA/RNA helicases (101247633), DEAD box helicase (DEAD30), and nucleolar protein (101250547). These proteins are involved in pre-RNA processing, RNA quality control and biogenesis of ribosomal subunits. The Al-down-regulated pseudouridine synthase (Solyc02g081810.2.1 annotated to TruB) catalyzes nucleotide pseudouridation and also serves as tRNA chaperone [60, 61]. A study on a truB gene disruptant (ΔtruB) strain of *Thermus thermophilus* showed that reducing protein synthesis of TruB affected synthesis of cold-shock proteins [62,63]. In the cluster, the TruB protein is associated with RPE1 (down-regulated), DEAD 30 (up-regulated), and nucleolar protein (101250547, down-regulated), which suggest that tRNA pseudouridation may play an important role in selective translation of these proteins in Al-treated cells. The LRR receptor-like serine/threonine-protein kinase protein (101262461) is involved in signal transduction with function in affecting endodermal cell fate in roots [64, 65]. The two Al-up-regulated glutathione S-transferases (GST, in cluster 1) and the association with cluster 13 (catalase, peroxidases) indicate a mechanism to protect the translation system from oxidative stress.

Cluster 3 contains two key enzymes for metabolism of lysine (101250089, dihydrodipicolinate synthase), arginine and proline (101261090, pyrroline-5-carboxylate reductase). The pyrroline-5-carboxylate reductase is associated with the threonine ammonia-lyase (Td), a key enzymes for biosynthesis of branched chain amino acids (BCAA) and subsequently to N-methyl-L-tryptophan oxidase (Solyc08g006430.2.1) which catalyzes the conversion of the non-proteogenic N-methyl-L-tryptophan to L-tryptophan (cluster 20). These interconnected-clusters indicate an Al-induced re-modulation of amino acid homeostasis.

Among all these inter-connected clusters, the RPE1 has the largest number of partners, and proteins such as Td, cat1 (catalase connecting with other antioxidant enzymes in clusters 13 and 18), 101248493 (mitochondrial phosphate carrier protein) (cluster 15, mitochondrial function). RPE1 is a RNA polymerase II which synthesizes mRNA and heterogeneous nuclear RNA (hnRNA). A study on mouse has demonstrated the role of RNA polymerase II in transcriptional reprogramming under stress conditions, such as a global loss of transcriptional termination due to an increase of RNA polymerase II occupancy downstream of mRNA genes under heat-stress [66]. In this study of Al-treated tomato TZ cells, changes in the abundance level of the RPE1 (and 101248465) and their associated proteins indicate an important role of these interactions in the development of stress transcriptomes and proteomes.

Clusters 4, 6, 7, 10, 11, 12, 16, 17, 19 are comprised each with 2-3 Al-up-regulated proteins. These clusters represent stress related proteins (clusters 19), cell wall remodeling (10, 12), protein post-translational modification and cellular protein quality control (clusters 6, 7), intracellular signal transduction and subcellular targeting of protein through secretory pathway (cluster 17). Proteins connecting these clusters and with other clusters were not identified which may be caused by the limitation of the STRING database where such proteins have not been annotated with relevant functions.

Analysis of the protein-protein interaction analysis revealed that proteins such as RPE1, DEAD 30, tRNA pseudouridine synthase B, and Td, are partners of multiple clusters of DEPs. The Al-induced changes in these proteins could impact a wide variety of biological processes in cell. Several proteins, such as FDH and GST, have been reported to affect Al-tolerance. The identification of these proteins in the Al-sensitive cells in the Al-tolerant tomato 'LA 2710' indicate a significant role of these proteins in Al tolerance. In the next step, the determination of the function of these proteins will advance our understanding of Al tolerance mechanisms.

4. Conclusions

In this study, we developed a high-throughput analysis of micro-dissected Al sensitive root cells, which yielded a deep proteome coverage (5780 proteins identified with high confidence and 3879 proteins quantified with ≥ 2 unique peptides) and revealed modification of

TZ cell proteomes under Al stress. According to functional pathways, KEGG pathways, and protein-protein association analysis, the quantified proteins are involved in all the major cellular processes. The differentially expressed proteins (DEPs) are comprised of 128 Al-up-regulated and 32 Al-down-regulated proteins. Cellular processes for transcription and protein translation are enriched with Al-down-regulated proteins. The Al-up-regulated proteins are involved in antioxidant and detoxification activity, proteasomes, cell wall remodeling, among others. This study has demonstrated the utility of LCM-TMT-proteomics approach for gaining biological insight into root TZ cells against Al stress. The technology developed herewith should now broadly enable deep spatially-resolved proteomics of tissues/organs with highly complex cell composition such as plant roots.

Supplementary Data

Fig. S1. Normal distribution of protein log2 fold of Al-treated versus non-Al treated tomato tissues.

Fig. S2. STRING Protein-protein association network constructed using differentially expressed proteins.

Table S1. List of quantified proteins and Al-induced differentially expressed proteins (DEPs) identified from epidermal and outer cortical cells in transition zone of Al-treated tomato root-tips (Excel file)

Table S2. List of KEGG pathways of quantified proteins from epidermal and outer cortical cells in transition zone of Al-treated tomato root-tips (Excel file)

Table S3. List of differentially expressed proteins from Al-treated to non-Al treated epidermal and outer cortical cells in the transition zone of tomato root tips

Table S4. Gene ontology (GO) terms of molecular function and cell components enriched with differentially expressed proteins analyzed using Plant MetGenMap (Excel file)

Table S5. List of proteins in the Pfam families identified using STRING analysis performed on differentially expressed proteins (Excel file)

Table S6. STRING MCL cluster of differentially expressed proteins (Excel File)

Table S7. Information of the Cytoscape STRING protein-protein interaction network (Excel file)

Acknowledgments

The authors wish to thank Johanna M. Dela Cruz, Carol J. Bayles of the Imaging Facility, Sheng Zhang of the Proteomics and Mass Spectrometry Facility, of the Cornell University Institute of Biotechnology for expert technical assistance and helpful discussions. This work was supported by 1890 Institution Teaching, Research and Extension Capacity Building Grants (CBG) Program, Award No. 2018-38821-27737, 2014-02868, and the Evans-Allen Research Funds for USDA-NIFA and ARS CRIS Projects 1907-21000-036/037-00D.

Disclaimer

Mention of trade names or commercial products in this publication is solely for the purpose of providing specific information and does not imply recommendation or endorsement by the US Department of Agriculture.

Notes

The authors declare no conflict of interest.

References

[1] D.L. Jones, E.B. Blancaflor, L.V. Kochian, S. Gilroy, Spatial coordination of aluminium uptake, production of reactive oxygen species, callose production and wall rigidification in maize roots, Plant Cell Environ. 29 (2006)1309–1318.

[2] C. Exley, M.J. Mold, The binding, transport and fate of aluminium in biological cells, J. Trace Elem. Med. Biol. 30 (2015) 90–95.

[3] B.L. Hartwell, F.R. Pember, Aluminum as a factor influencing the effect of acid soils on different crops, J. Am. Soc. Agron. 10 (1918) 45–47.

[4] L.V. Kochian, O.A. Hoekenga, M.A.Pineros, How do crop plants tolerate acid soils? Mechanisms of aluminum tolerance and phosphorous efficiency, Annu. Rev. Plant. Biol. 55 (2004) 459–493.

[5] J. Liu, M.A. Piñeros, L.V. Kochian, The role of aluminum sensing and signaling in plant aluminum resistance, J. Integr. Plant Biol. 56 (2014)221–230.

[6] W.J. Horst, W. Yunxia, E. Dejene, The role of the root apoplast in aluminium-induced inhibition of root elongation and in aluminium resistance of plants: a review, Ann. Bot. 106 (2010)185–197.

[7] P.R. Ryan, M. Skerrett, G.P. Findlay, E. Delhaize, S.D. Tyerman, Aluminum activates an anion channel in the apical cells of wheat roots, Proc. Nat. Acad. Sci. 94 (1997) 6547–6552.

[8] W. Cajero Sánchez, B. García-Ponce, M.P. Sánchez, E.R. Álvarez-Buylla, A. Garay-Arroyo, 2017. Identifying the transition to the maturation zone in three ecotypes of Arabidopsis thaliana roots, Commun. Integr. Biol. 11(1), e1395993. https://doi: 10.1080/19420889.2017.1395993.

[9] M. Sivaguru, W.J. Horst, The distal part of the transition zone is the most aluminium-sensitive apical root zone of *Zea mays* L, Plant Physiol.116 (1998) 155–163.

[10] J.P. Verbelen, T. De Cnodder, J. Le, K. Vissenberg, F. Baluška, The root apex of *Arabidopsis thaliana* consists of four distinct zones of growth activities, Plant Signal. Behav. 1 (2006) 296–304.

[11] F. Baluška, S. Mancuso, 2013. Root apex transition zone as oscillatory zone, Front. Plant Sci. 4,354. http://doi: 10.3389/fpls.2013.00354.

[12] M. Kollmeier, H.H. Felle, W.J. Horst, Genotypical differences in aluminum resistance of maize are expressed in the distal part of the transition zone. Is reduced basipetal auxin flow involved in inhibition of root elongation by aluminum?, Plant Physiol. 122 (2000) 945–956.

563 [13] M. Kollmeier, P. Dietrich, C.S. Bauer, W.J. Horst, R. Hedrich, Aluminum activates a
564 citrate-permeable anion channel in the aluminum-sensitive zone of the maize root apex. A
565 comparison between an aluminum- sensitive and an aluminum-resistant cultivar, Plant Physiol.
566 126 (2001) 397–410.

567 [14] P. Illés, M. Schlicht, J. Pavlovkin, I. Lichtscheidl, F. Baluska, M. Ovecka, Aluminium
568 toxicity in plants: internalization of aluminium into cells of the transition zone in Arabidopsis
569 root apices related to changes in plasma membrane potential, endosomal behaviour, and nitric
570 oxide production, J. Exp. Bot. 57 (2006) 4201–4213.

571 [15] M. Sivaguru, F. Baluška, D. Volkmann, H.H. Felle, W. J. Horst, Impacts of aluminum on
572 the cytoskeleton of the maize root apex. short-term effects on the distal part of the transition
573 zone, Plant Physiol. 119 (1999) 1073–1082.

574 [16] M. Sivaguru, J. Liu, L.V. Kochian, Targeted expression of SbMATE in the root distal
575 transition zone is responsible for sorghum aluminum resistance, Plant J. 76 (2013)297–307.

576 [17] X. Kong, G. Liu, J. Liu, Z. Ding, The root transition zone: A hot spot for signal crosstalk,
577 Trends Plant Sci. 23 (2018) 403–409.

578 [18] R. Di Mambro, M. De Ruvo, E. Pacifici, E. Salvi, R. Sozzani, P.N. Benfey, W. Busch, O.
579 Novak, K. Ljung, L. Di Paola, A.F.M. Marée, P. Costantino, V.A. Grieneisen, A. Sabatini,
580 Auxin minimum triggers the developmental switch from cell division to cell differentiation in the
581 Arabidopsis root, Proc. Natl. Acad. Sci. USA. 114 (2017) E7641–E7649.

582 [19] P. Sun, Q.Y. Tian, J. Chen, W.H. Zhang, Aluminium-induced inhibition of root elongation
583 in Arabidopsis is mediated by ethylene and auxin, J. Exp. Bot. 61 (2010) 347–356.

584 [20] G. Clair, P.D. Piehowski, T. Nicola, J.A. Kitzmiller, E.L. Huang, E.M. Zink, R. L. Sontag,
585 D.J. Orton, R.J. Moore, J.P. Carson, R.D. Smith, J.A. Whitsett, R.A. Corley, N. Ambalavanan,
586 C. Ansong, 2016. Spatially-resolved proteomics: Rapid quantitative analysis of laser capture
587 microdissected alveolar tissue samples, Sci. Rept. 6, 39223. https://doi.org/10.1038/srep39223

588 [21] Y. Liang, Y. Zhu, M. Dou, K. Xu, R.K. Chu, W.B. Chrisler, R. Zhao, K.K. Hixson, R.T.
589 Kelly, Spatially resolved proteome profiling of <200 cells from tomato fruit pericarp by
590 integrating laser-capture microdissection with nanodroplet sample preparation, Anal. Chem. 90
591 (2018)11106–11114.

592 [22] A.J. Matas, T.H. Yeats, G.J. Buda, Y. Zheng, S. Chatterjee, T. Tohge, L. Ponnala, A. Adato,
593 A. Aharoni, R. Stark, A.R. Fernie, Z. Fei, J.J. Giovannoni, J.K. Rose, Tissue- and cell-type
594 specific transcriptome profiling of expanding tomato fruit provides insights into metabolic and
595 regulatory specialization and cuticle formation, Plant Cell 23 (2011) 3893–3910.

596 [23] Y.D. Zhu, H. Li, S. Bhatti, S. Zhou, Y. Yang, T. Fish, T.W. Thannhauser, 2016.
597 Development of a laser capture microscope-based single-cell-type proteomics tool for studying

598 proteomes of individual cell layers of plant roots, Hort. Res. 3,16026.
599 https://doi.org/10.1038/hortres.2016.26

600 [24] Tomato Genetics Resource Center. Accession Details: Accession: LA2710.
601 https://tgrc.ucdavis.edu/Misc-stocks%20list%202015.pdf, 2019 (accessed 04 September, 2019).

602 [25] J. Shaff, B. Schultz, E.J. Craft, R. Clark, L.V. Kochian, GEOCHEM-EZ: a chemical
603 speciation program with greater power and flexibility, Plant Soil J. 330 (2010) 207–214.

604 [26] E. Polle, C.F. Konzak, J.A. Kittrick, Visual detection of aluminum tolerance levels in wheat
605 by hematoxylin staining, Crop Sci. 18 (1978) 823–827.

606 [27] J.D. Ownby, Mechanisms of reaction of hematoxylin with aluminium-treated wheat
607 roots, Physiol. Planta. 87(1993): 371–380.

608 [28] B. Ezaki, R.C. Gardner, Y. Ezaki, H. Matsumoto, Expression of aluminum-induced genes
609 in transgenic arabidopsis plants can ameliorate aluminum stress and/or oxidative stress, Plant
610 Physiol. 122 (2000) 657–665.

611 [29] H. Li, Y. Zhu, M. Rangu, X. Wu, S. Bhatti, S. Zhou, Y. Yang, T. Fish, T.W. Thannhauser,
612 2018. Identification of heat-induced proteomes in tomato microspores using LCM-proteomics
613 analysis, Single Cell Biol. 7,173. http://doi: 10.4172/2168-9431.1000173

614 [30] M. Rangu, Z. Ye, S. Bhatti, S. Zhou, Y. Yang, T. Fish, T.W. Thannhauser, 2018.
615 Association of proteomics changes with Al-sensitive root zones in Switchgrass, Proteomes 6, 15.
616 http://doi: 10.3390/proteomes6020015.

617 [31] S. Zhou, I. Okekeogbu, S. Sangireddy, Z. Ye, H. Li, S. Bhatti, D. Hui, D.W. McDonald, Y.
618 Yang, S. Giri, K.J. Howe, T. Fish, T.W. Thannhauser, Proteome modification in tomato plants
619 upon long-term aluminum treatment, J. Proteome Res. 15 (2016) 1670–1684.

620 [32] J.G. Joung, A.M. Corbett, S.M. Fellma, D.M. Tieman, H.J. Klee, J.J. Giovannoni, Z. Fei,
621 Plant MetGenMAP: An integrative analysis system for plant systems biology, Plant Physiol. 151
622 (2009)1758–1768.

623 [33] D. Szklarczyk, J.H. Morris, H. Cook, M. Kuhn, S. Wyder, M. Simonovic, A. Santos, N.T.
624 Doncheva, A. Roth, P. Bork, L.J. Jensen, C. von Mering, The STRING database in 2017:
625 quality-controlled protein-protein association networks, made broadly accessible, Nucleic Acids
626 Res. 45 (2017) D362–D368.

627 [34] R. Stryiński, J. Mateos, S. Pascual, A.F. González, J.M. Gallardo, E. Łopieńska-Biernat, I.
628 Medina, M. Carrera, Proteome profiling of L3 and L4 Anisakis simplex development stages by
629 TMT-based quantitative proteomics, J. Proteomics 201 (2019)1–11.

[35] P. Shannon, A. Markiel, O. Ozier, N.S. Baliga, J.T. Wang, D. Ramage, N. Amin, B. Schwikowski, T. Ideker, Cytoscape: a software environment for integrated models of biomolecular interaction networks, Genome Res.13 (2003) 2498–2504.

[36] V.M. Achary, N.L. Parinandim, B.B. Panda, Aluminum induces oxidative burst, cell wall NADH peroxidase activity, and DNA damage in root cells of *Allium cepa* L, Environ. Mol. Mutagen. 53 (2012) 550–560.

[37] H. Matsumoto, H. Motoda, Aluminum toxicity recovery processes in root apices. Possible association with oxidative stress, Plant Sci. 185–186 (2012)1–8.

[38] D. Dembinsky, K. Woll, M. Saleem, Y. Liu, Y. Fu, L.A. Borsuk, T. Lamkemeyer, C. Fladerer, J. Madlung, B. Barbazuk, A. Nordheim, D. Nettleton, P.S. Schnable, F. Hochholdinger, Transcriptomic and proteomic analyses of pericycle cells of the maize primary root, Plant Physiol. 145 (2007) 575–588.

39. M. Thapa, A. Bommakanti, M. Shamsuzzaman, B. Gregory, L. Samsel, J.M. Zengel, L. Lindahl, Repressed synthesis of ribosomal proteins generates protein-specific cell cycle and morphological phenotypes, Mol. Biol. Cell 24 (2013) 3620–3633.

[40] S. Zhou, R. Sauvé, T.W. Thannhauser, Proteome changes induced by aluminium stress in tomato roots, J. Expt. Bot. 60 (2009) 1849–1857.

[41] S. Zhou, R. Sauvé, Z. Liu, S. Reddy, S. Bhatti, S.D. Hucko, T. Fish, T.W. Thannhauser, Identification of salt-induced changes in leaf and root proteomes of the wild tomato, *Solanum chilense*, J. Amer. Soc. Hort. Sci. 136 (2011) 288–302.

[42] U. Topf, I. Suppanz, L. Samluk, L. Wrobel, A. Böser, P. Sakowska, B. Knapp, M.K. Pietrzyk, A. Chacinska, B. Warscheid, Quantitative proteomics identifies redox switches for global translation modulation by mitochondrially produced reactive oxygen species, Nature Commun. 9 (2018) 324.

[43] B. Liu, S.B. Qian, Translational reprogramming in cellular stress response, Wiley Interdiscip. Rev. RNA 5 (2014) 301–315.

[44] D.E. Andreev, P.B. O'Connor, G. Loughran, S.E. Dmitriev, P.V. Baranov, I.N. Shatsky, Insights into the mechanisms of eukaryotic translation gained with ribosome profiling, Nucleic Acids Res. 45 (2017) 513–526.

[45] M.V. Rodnina, The ribosome in action: Tuning of translational efficiency and protein folding, Protein Sci. 25 (2016) 1390–1406.

[46] Y. Gonskikh, N. Polacek, Alterations of the translation apparatus during aging and stress response, Mech. Ageing Dev. 168 (2017) 30–36.

[47] A.O. Sousa, E.T. Assis, C.P. Pirovani, F.C. Alvim, M.G. Costa, Phosphate-induced-1 gene from Eucalyptus (EgPHI-1) enhances osmotic stress tolerance in transgenic tobacco, Genet. Mol. Res. 13 (2014)1579–1588.

[48] C.Q. Quan, Z.G. Bai, S.W. Zheng, J.M. Zhou, Q. Yu, Z.J. Xu, X.L. Gao, L.H. Li, J.Q. Zhu, X.M. Jia, R.J. Chen, Genome-wide analysis and environmental response profiling of phosphate-induced-1 family genes in rice (*Oryza sativa*), Biotechn. Biotechn. Equip. 33 (2019) 627–638.

[49] A. Sharma, B. Shahzad, A. Rehman, R. Bhardwaj, M. Landi, B. Zheng, 2019. Response of phenylpropanoid pathway and the role of polyphenols in plants under abiotic stress, Molecules 24(13), pii: E2452. https://doi: 10.3390/molecules24132452.

[50] N. Silva VE, P. Mazzafera, I. Cesarino, 2019. Should I stay or should I go: are chlorogenic acids mobilized towards lignin biosynthesis?, Phytochemistry 166, 112063. https://doi: 10.1016/j.phytochem.2019.112063.

[51] T. Vogt. Phenylpropanoid biosynthesis, Mol. Plant 3(2010) 2–20.

[52] D. Giordano, S. Provenzano, A. Ferrandino, M. Vitali, C. Pagliarani, F. Roman, F. Cardinale, S.D. Castellarin, A. Schubert, Characterization of a multifunctional caffeoyl-CoA O-methyltransferase activated in grape berries upon drought stress, Plant Physiol. Biochem.101 (2016) 23–32.

[53] M. Sivaguru, T. Fujiwara, J. Samaj, F. Baluska, Z. Yang, H. Osawa, T. Maeda, T. Mori, D. Volkmann, H. Matsumoto, Aluminum-induced 1->3-beta-D-glucan inhibits cell-to-cell trafficking of molecules through plasmodesmata. A new mechanism of aluminum toxicity in plants, Plant Physiol. 124 (2000) 991–1006.

[54] N. Massot, M. Llugany, C. Poschenrieder, J.Barceló, Callose production as indicator of aluminum toxicity in bean cultivars, J. Plant Nutr. 22 (1999)1–10.

[55] A.A. Dmitriev, G.S. Krasnov, T.A. Rozhmina, N.V. Kishlyan, A.V. Zyablitsin, A.F. Sadritdinova, A.V. Snezhkina, M.S. Fedorova, O.Y. Yurkevich, O.V. Muravenko, N.L. Bolsheva, A.V. Kudryavtseva, N.V. Melnikova, 2016. Glutathione S-transferases and UDP-glycosyltransferases are involved in response to aluminum stress in flax, Front. Plant Sci.7, 1920. https://doi: 10.3389/fpls.2016.01920.

[56] K. L. Gorres, R.T. Raines, Prolyl 4-hydroxylase, Crit. Rev. Biochem. Mol. Biol. 45 (2010) 106–124.

[57] J. Liesivuori, H. Savolainen, Methanol and formic acid toxicity: biochemical mechanisms, Pharmacol. Toxicol. 69 (1991)157–163.

[58] R. Li, M. Moore, P.C. Bonham-Smith, J. King, Overexpression of formate dehydrogenase in Arabidopsis thaliana resulted in plants tolerant to high concentrations of formate, J. Plant Physiol. 159 (2002)1069–1076.

[59] H.Q. Lou, Y.L. Gong, W. Fan, J.M. Xu, Y. Liu, M.J. Cao, M.H. Wang, J.L. Yang, S.J. Zheng, A formate dehydrogenase confers tolerance to aluminum and low pH, Plant Physiol. 171(2016) 294–305.

[60]A.C. Rintala-Dempsey, U. Kothe, Eukaryotic stand-alone pseudouridine synthases - RNA modifying enzymes and emerging regulators of gene expression?, RNA Biol. 14 (2017) 1185–1196.

[61]F. Spenkuch, Y. Motorin, M. Helm, Pseudouridine: still mysterious, but never a fake (uridine)!, RNA Biol. 11 (2014) 1540–1554.

[62] L.C. Keffer-Wilkes, G.R. Veerareddygari, U. Kothe, RNA modification enzyme TruB is a tRNA chaperone, Proc. Natl. Acad. Sci. USA 113 (2016) 14306–14311.

[63] K. Ishida, T. Kunibayashi, C. Tomikawa, A. Ochi, T. Kanai, A. Hirata, C. Iwashita, H. Hori, Pseudouridine at position 55 in tRNA controls the contents of other modified nucleotides for low-temperature adaptation in the extreme-thermophilic eubacterium *Thermus thermophiles*, Nucleic Acids Res. 39 (2011) 2304–2318.

[64] A.J. Afzal, A.J. Wood, D.A. Lightfoot, Plant receptor-like serine threonine kinases: roles in signaling and plant defense, Mol. Plant Microbe Interact. 21 (2008) 507–517.

[65] A. Pfister, M. Barberon, J. Alassimone, L. Kalmbach, Y. Lee, J.E. Vermeer, M. Yamazaki, G. Li, C. Maurel, J. Takano, T. Kamiya, D.E Salt, D. Roppolo, N. Geldner, 2014. A receptor-like kinase mutant with absent endodermal diffusion barrier displays selective nutrient homeostasis defects, Elife 3,e03115. https://doi: 10.7554/eLife.03115.

[66] J.F. Cardiello, J.A. Goodrich, J.F. Kugel, 2018. Heat shock causes a reversible increase in RNA polymerase II occupancy downstream of mRNA genes, consistent with a global loss in transcriptional termination, Mol. Cell Biol.38(18), pii: e00181-118. http://doi: 10.1128/MCB.00181-18.

729

730

731

732

733

734

735

736 **Table 1**

737 The list of KEGG pathways of Al-induced differentially expressed proteins in epidermal and
738 outer cortical cells at transition zone of tomato root-tips.

KEGG term ID[a]	Term description[b]	Protein accession[c]	Log2Fold (T/C)[d]	Protein description[e]
sly00940	Phenylpropanoid biosynthesis	Solyc01g105590.2.1	0.66	Hydroxycinnamoyl CoA quinate transferase
		Solyc02g094180.2.1	0.77	Peroxidase 1
		Solyc03g119080.2.1	0.84	Beta-glucosidase
		Solyc01g105070.2.1	0.88	Peroxidase
		Solyc10g050160.1.1	0.97	Caffeoyl-CoA 3-O-methyltransferase
		Solyc07g052510.2.1	1.09	Peroxidase
		Solyc05g046010.2.1	1.20	Peroxidase
		Solyc02g079500.2.1	1.24	Peroxidase
		Solyc00g072400.2.1	1.26	Peroxidase 1
		Solyc10g076240.1.1	1.62	Peroxidase 1
		Solyc03g006700.2.1	1.86	Peroxidase
		Solyc05g052280.2.1	1.97	Peroxidase
		Solyc10g076220.1.1	1.99	Peroxidase 1
		Solyc02g084790.2.1	2.08	Peroxidase
		Solyc02g084780.2.1	2.14	Peroxidase
sly00480	Glutathione metabolism	Solyc09g011600.2.1	0.66	Glutathione S-transferase

		Solyc09g011630.2.1	0.75	Glutathione S-transferase
		Solyc10g084400.1.1	0.91	Glutathione S-transferase
		Solyc09g011520.2.1	0.99	Glutathione S-transferase
		Solyc09g011590.2.1	1.23	Glutathione S-transferase
		Solyc12g056250.1.1	1.29	Glutathione S-transferase
		Solyc07g056480.2.1	1.45	Glutathione S-transferase
		Solyc09g074850.2.1	1.61	Glutathione S-transferase
sly01100	Metabolic pathways	Solyc08g006430.2.1	-0.87	N-methyl-L-tryptophan oxidase
		Solyc10g055810.1.1	-0.75	Endochitinase
		Solyc03g044660.2.1	-0.74	Dihydrodipicolinate synthase
		Solyc02g068640.2.1	-0.72	Pyrroline-5-carboxylate reductase
		Solyc01g105070.2.1	-0.71	Nucleolar protein
		Solyc03g063600.2.1	0.66	Guanylate kinase
		Solyc01g105590.2.1	0.66	Hydroxycinnamoyl CoA quinate transferase
		Solyc04g049330.2.1	0.68	V-type proton ATPase
		Solyc02g067530.2.1	0.72	Prolyl 4-hydroxylase
		Solyc02g094180.2.1	0.77	Peroxidase 1
		Solyc10g007960.1.1	0.78	Allene oxide synthase
		Solyc02g086880.2.1	0.81	Formate dehydrogenase
		Solyc06g075810.2.1	0.82	NADH dehydrogenase
		Solyc03g119080.2.1	0.84	Beta-glucosidase
		Solyc05g054060.2.1	0.84	UTP-glucose 1 phosphate uridylyltransferase
		Solyc10g050160.1.1	0.97	Caffeoyl-CoA 3-O-methyltransferase
		Solyc07g052510.2.1	1.09	Peroxidase
		Solyc09g008670.2.1	1.13	Threonine ammonia-lyase
		Solyc05g046010.2.1	1.20	Peroxidase
		Solyc02g079500.2.1	1.24	Peroxidase
		Solyc00g072400.2.1	1.26	Peroxidase 1
		Solyc07g007550.2.1	1.31	Heparanase
		Solyc03g025720.2.1	1.47	Long-chain-fatty-acid-CoA ligase
		Solyc10g076240.1.1	1.62	Peroxidase 1
		Solyc03g006700.2.1	1.86	Peroxidase

		Solyc05g052280.2.1	1.97	Peroxidase
		Solyc10g076220.1.1	1.99	Peroxidase 1
		Solyc02g084790.2.1	2.08	Peroxidase
		Solyc02g084780.2.1	2.14	Peroxidase
sly01110	Biosynthesis of secondary metabolites	Solyc03g044660.2.1	-0.74	Dihydrodipicolinate synthase
		Solyc02g068640.2.1	-0.72	Pyrroline-5-carboxylate reductase
		Solyc01g105590.2.1	0.66	Hydroxycinnamoyl CoA quinate transferase
		Solyc02g094180.2.1	0.77	Peroxidase 1
		Solyc10g007960.1.1	0.78	Allene oxide synthase
		Solyc03g119080.2.1	0.84	Beta-glucosidase
		Solyc10g050160.1.1	0.97	Caffeoyl-CoA 3-O-methyltransferase
		Solyc01g105070.2.1	1.01	Inosine-uridine preferring nucleoside hydrolase
		Solyc07g052510.2.1	1.09	Peroxidase
		Solyc12g094620.1.1	1.09	Catalase
		Solyc09g008670.2.1	1.13	Threonine ammonia-lyase
		Solyc05g046010.2.1	1.20	Peroxidase
		Solyc02g079500.2.1	1.24	Peroxidase
		Solyc00g072400.2.1	1.26	Peroxidase 1
		Solyc10g076240.1.1	1.62	Peroxidase 1
		Solyc03g006700.2.1	1.86	Peroxidase
		Solyc05g052280.2.1	1.97	Peroxidase
		Solyc10g076220.1.1	1.99	Peroxidase 1
		Solyc02g084790.2.1	2.08	Peroxidase
		Solyc02g084780.2.1	2.14	Peroxidase
sly00591	Linoleic acid metabolism	Solyc08g029000.2.1	0.75	Lipoxygenase
		Solyc08g014000.2.1	0.80	Lipoxygenase
sly00630	Glyoxylate and dicarboxylate metabolism	Solyc02g086880.2.1	0.81	Formate dehydrogenase
		Solyc12g094620.1.1	1.09	Catalase
		Solyc03g025720.2.1	1.47	Long-chain-fatty-acid-CoA ligase

739 [a]The identifier in reference KEGG pathway of *Solanum lycopersicum.*

740 [b]Name of the KEGG pathway enriched with the tomato proteins.

741 [c]Accession number in the International Tomato Annotation Group (ITAG3.20) protein database.

742 [d]Log2 transformed abundance ratio of Al-treated (T) and non-treated groups (C) in the PD2.2

743 report.

744 [e]Annotated proteins in tomato genome database

745

Figure legends.

Fig.1. Determination of the Al-sensitive root-tip zone and cell layers in tomato roots. A,B, whole root staining; C,D, 10 µm thick frozen sections of root tips.

A: Accumulation of reactive oxygen species (ROS) shown by green fluorescence on Al-treated root-tips stained with 2',7'-dichlorofluorescin diacetate (DCFDA). Overlay (Left) and fluorescence (Right) images are shown individually. The fluorescent images were taken using an excitation filter BP 450-490 and an emission filter BP 500-550.

B: Hematoxylin stained root-tips imaged under bright field, showing the Al-treated root-tip stained with darker color due to Al accumulation.

C, Microsection of non-Al treated root-tips stained with hematoxylin, showing the consistent and light colored root section.

D, Microsection of Al-treated root-tips stained with hematoxylin, showing the darker stained outer layers of the transition zone tissue.

Images A, C, D were taken using a ZEISS M2 Apotome.2 Imager; image B under an Olympus fluorescence stereomicroscope.

Fig. 2 The distribution of quantified proteome identified from Al-treated tomato root tips using laser capture microdissection (LCM) - tandem mass tag (TMT) - proteomics analysis. The majority of the proteins were quantified with 2-5/6 peptides, and only a few proteins were identified with more than 10 peptides. Inserted images (arrow pointed within the circles) showing the epidermal and outer-cortical tissues of transition zone before and after captured using LCM.

Fig. 3. KEGG pathways identified using STRING analysis performed on quantified proteins from epidermal and cortical cells in transition zones of root-tips from Al-treated tomatoes. The percentage of identified proteins compared to the number of proteins in annotated tomato genome was shown. A: Metabolic pathways; B: Genetic information process

Fig. 4. Categories of molecular function (A) and cell component (B) classified using the Plant MetGenMap analysis performed on differentially expressed proteins in epidermal and outer

777 cortical cells in root transition zone of Al-treated tomatoes. The GO term for each category was
778 provided in the bracket. Some of the proteins are placed in more than one categories. The
779 negative number indicates Al-down-regulated proteins.
780 **Fig.5.** Pfam family of Al-induced differential expressed proteins in tomato root tips.
781 **Fig.6.** Cytoscape image of protein-protein interaction network constructed using STRING
782 analysis performed on Al-induced differentially expressed proteins identified from epidermal and
783 outer cortical cells in transition zones of root-tips from Al-treated tomatoes. The circles in red
784 color indicate Al-up-regulated proteins, and circles in blue indicate Al-down-regulated proteins.
785 The depth of the color corresponds to the protein Log_2Fold change between Al-treated to non-Al-
786 treated control groups.

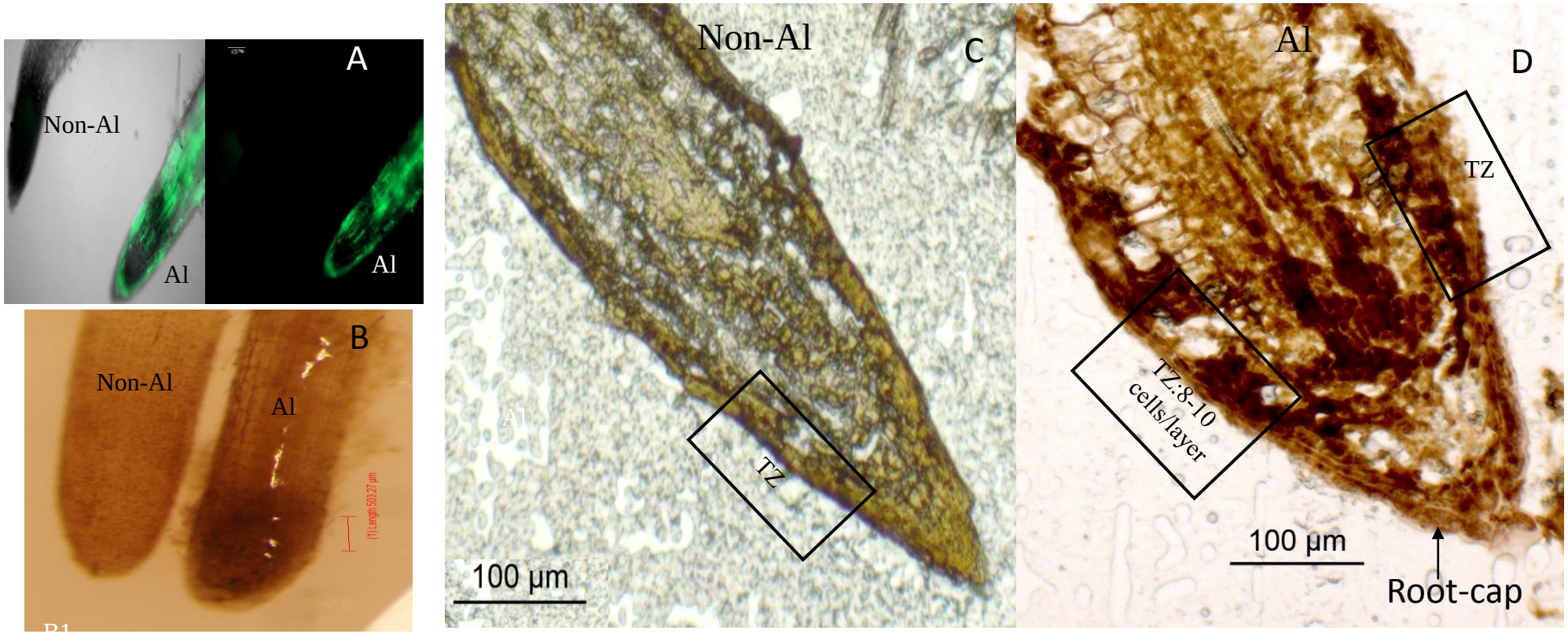

Fig.1 Determination of the Al-sensitive root-tip zone and cell layers in tomato roots. A,B, whole root staining; C,D, 10 µm thick frozen sections of root tips.

A: Accumulation of reactive oxygen species (ROS) shown by green fluorescence on Al-treated root-tips stained with 2',7'-dichlorofluorescin diacetate (DCFDA). Overlay (Left) and fluorescence (Right) images are shown individually. The fluorescent images were taken using an excitation filter BP 450-490 and an emission filter BP 500-550.
B: Hematoxylin stained root-tips imaged under bright field, showing the Al-treated root-tip stained with darker color due to Al accumulation.
C, Microsection of non-Al treated root-tips stained with hematoxylin, showing the consistent and light colored root section.
D, Microsection of Al-treated root-tips stained with hematoxylin, showing the darker stained outer layers of the transition zone tissue.
Images A, C, D were taken using a ZEISS M2 Apotome.2 Imager; image B under an Olympus fluorescence stereomicroscope.

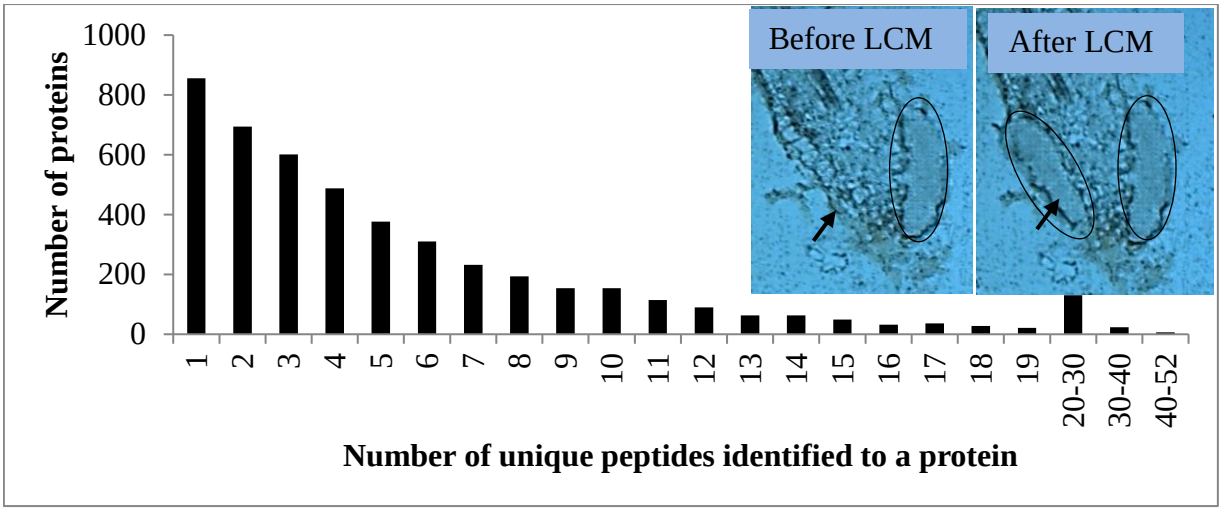

Fig. 2. The distribution of quantified proteome identified from Al-treated tomato root tips using laser capture microdissection (LCM)-tandem mass tag (TMT)-proteomics analysis. A majority of the proteins were quantified with 2-5/6 peptides, and only a few proteins were identified with more than 10 peptides. Inserted images (arrows pointed to the circles) showing the epidermal and outer cortical cells in root-tip transition zone before and after capture using LCM.

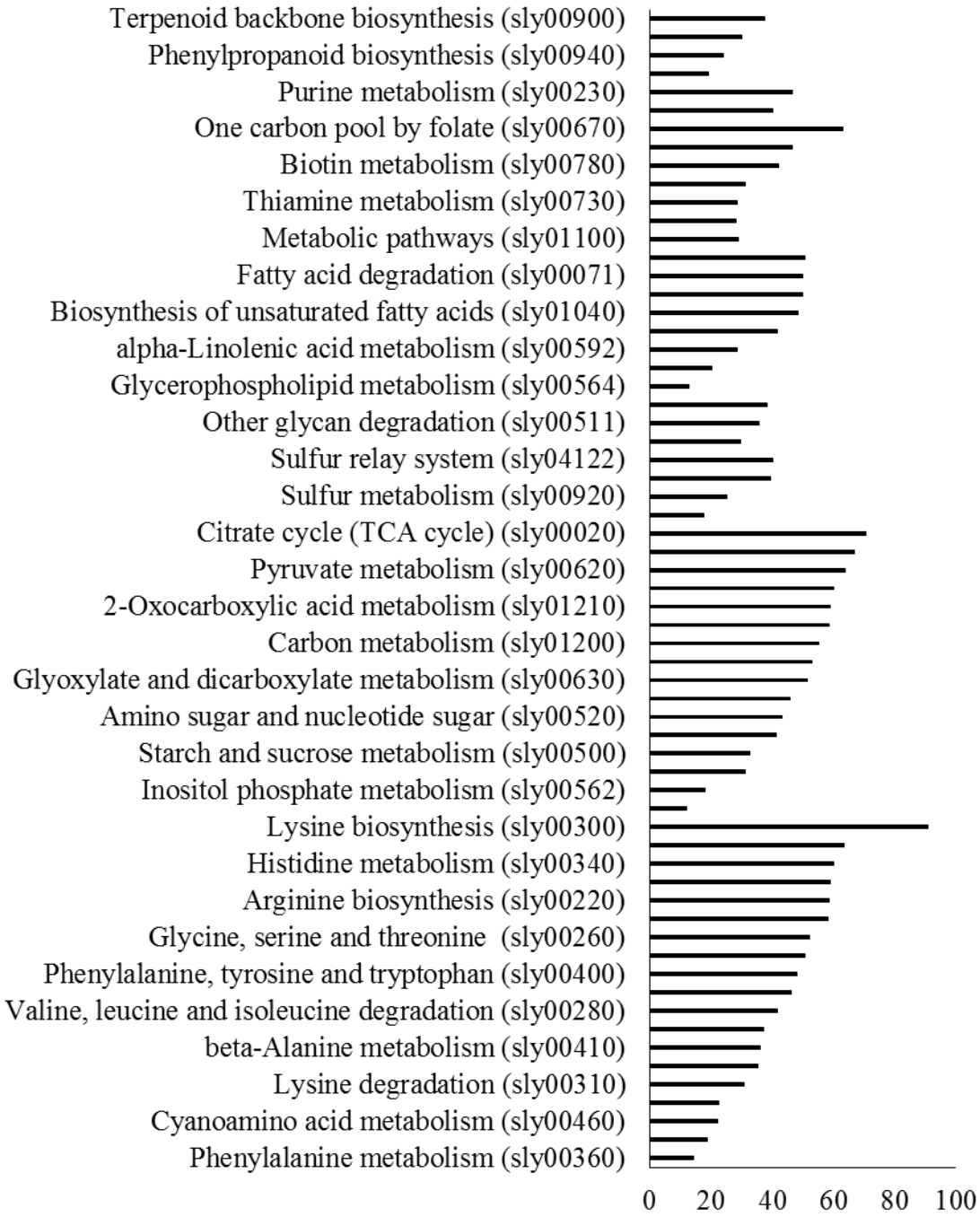
Terpenoid backbone biosynthesis (sly00900)
Phenylpropanoid biosynthesis (sly00940)
Purine metabolism (sly00230)
One carbon pool by folate (sly00670)
Biotin metabolism (sly00780)
Thiamine metabolism (sly00730)
Metabolic pathways (sly01100)
Fatty acid degradation (sly00071)
Biosynthesis of unsaturated fatty acids (sly01040)
alpha-Linolenic acid metabolism (sly00592)
Glycerophospholipid metabolism (sly00564)
Other glycan degradation (sly00511)
Sulfur relay system (sly04122)
Sulfur metabolism (sly00920)
Citrate cycle (TCA cycle) (sly00020)
Pyruvate metabolism (sly00620)
2-Oxocarboxylic acid metabolism (sly01210)
Carbon metabolism (sly01200)
Glyoxylate and dicarboxylate metabolism (sly00630)
Amino sugar and nucleotide sugar (sly00520)
Starch and sucrose metabolism (sly00500)
Inositol phosphate metabolism (sly00562)
Lysine biosynthesis (sly00300)
Histidine metabolism (sly00340)
Arginine biosynthesis (sly00220)
Glycine, serine and threonine (sly00260)
Phenylalanine, tyrosine and tryptophan (sly00400)
Valine, leucine and isoleucine degradation (sly00280)
beta-Alanine metabolism (sly00410)
Lysine degradation (sly00310)
Cyanoamino acid metabolism (sly00460)
Phenylalanine metabolism (sly00360)
0
20
40
60
80
100
% of identified proteins in the annoated tomato genome

A

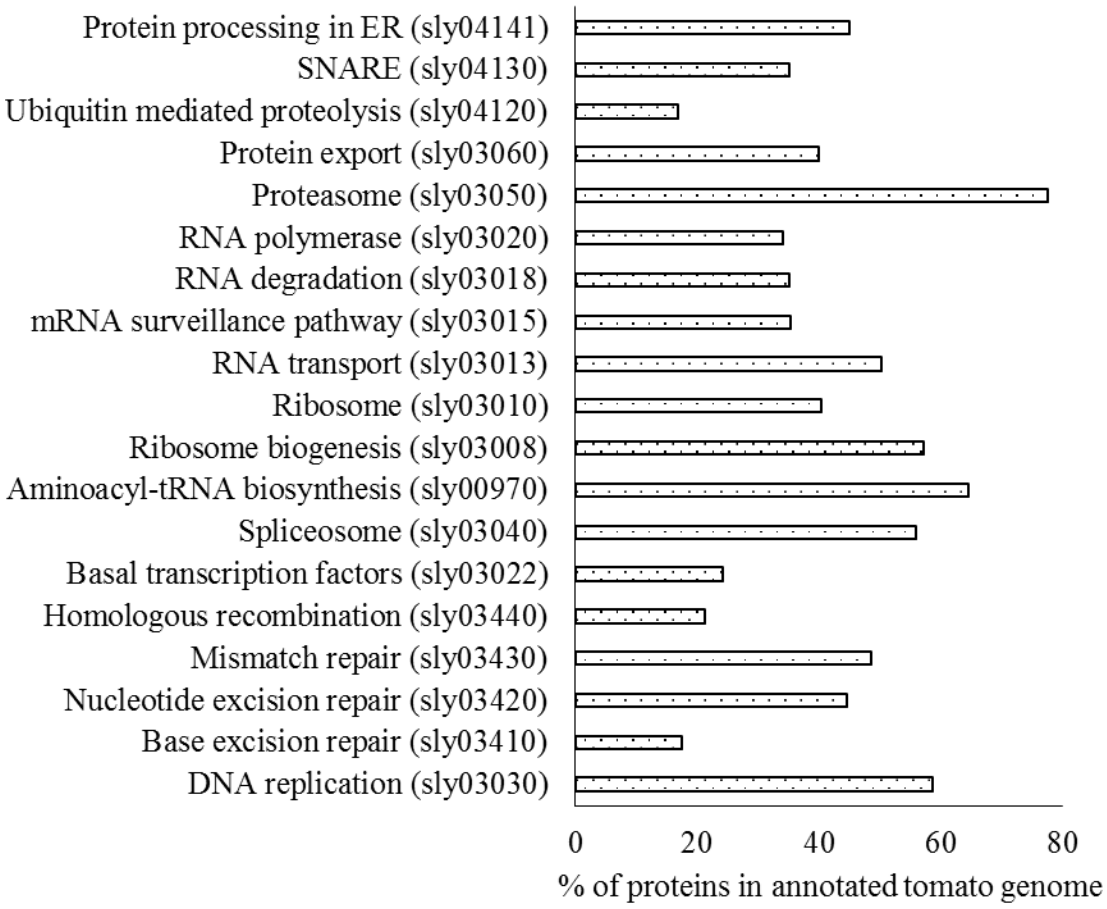

B

Fig. 3. KEGG pathways identified using STRING analysis performed on quantified proteins from epidermal and cortical cells in root tip transition zones of Al-treated tomatoes. The percentage of identified proteins compared to the number of proteins in annotated tomato genome was shown. A: Metabolic pathways; B: Genetic information process

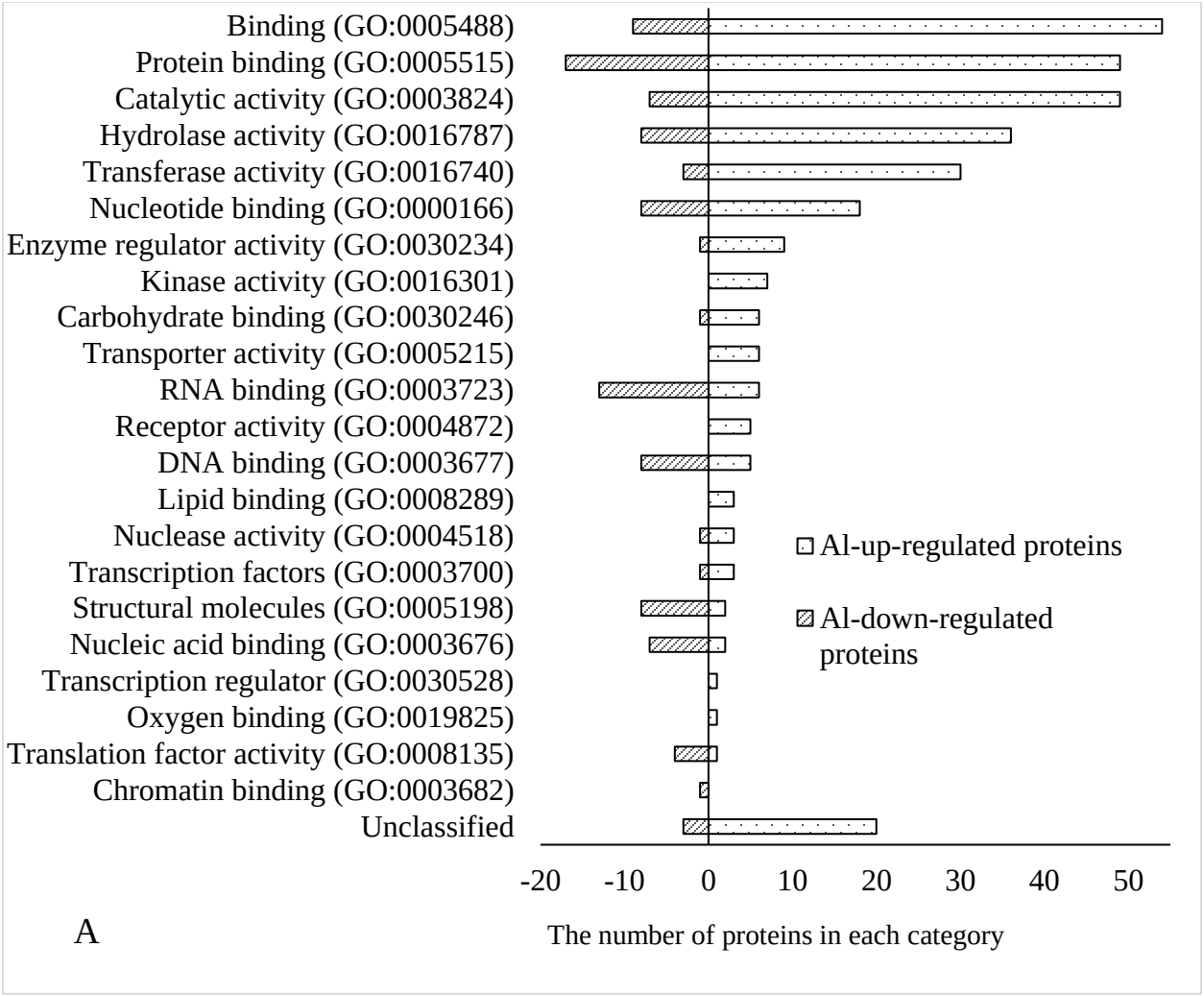
Binding (GO:0005488)
Protein binding (GO:0005515)
Catalytic activity (GO:0003824)
Hydrolase activity (GO:0016787)
Transferase activity (GO:0016740)
Nucleotide binding (GO:0000166)
Enzyme regulator activity (GO:0030234)
Kinase activity (GO:0016301)
Carbohydrate binding (GO:0030246)
Transporter activity (GO:0005215)
RNA binding (GO:0003723)
Receptor activity (GO:0004872)
DNA binding (GO:0003677)
Lipid binding (GO:0008289)
Nuclease activity (GO:0004518)
Transcription factors (GO:0003700)
Structural molecules (GO:0005198)
Nucleic acid binding (GO:0003676)
Transcription regulator (GO:0030528)
Oxygen binding (GO:0019825)
Translation factor activity (GO:0008135)
Chromatin binding (GO:0003682)
Unclassified
Al-up-regulated proteins
Al-down-regulated proteins
-20
-10
0
10
20
30
40
50
The number of proteins in each category

A

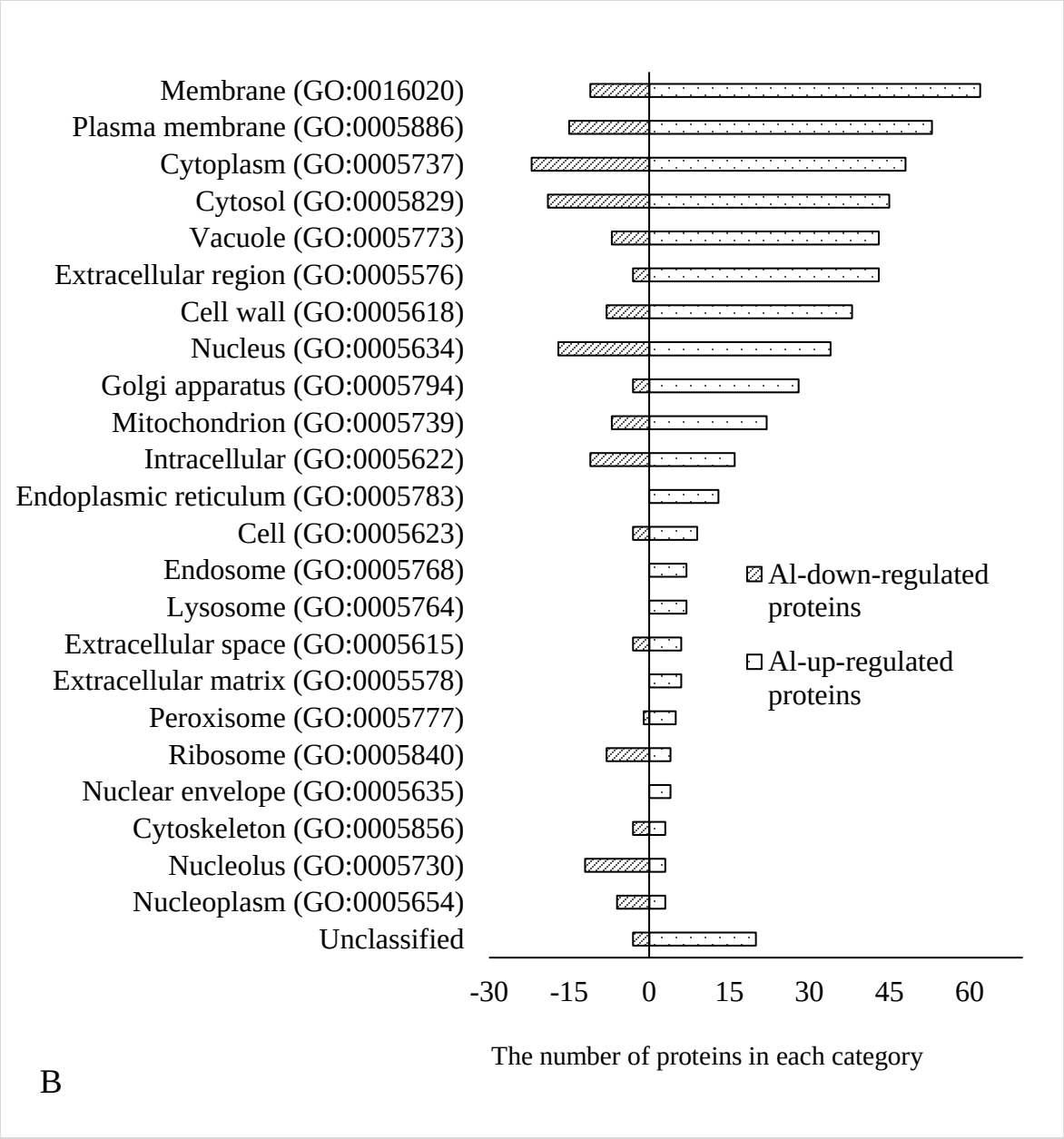

Fig. 4. Categories of molecular function (A) and cell component (B) classified using the Plant MetGenMap analysis performed on differentially expressed proteins in epidermal and outer cortical cells in root transitional zone of Al-treated tomatoes. The GO term for each category was provided in the bracket. Some of the proteins are placed in more than one category. The negative number indicates Al-down-regulated proteins.

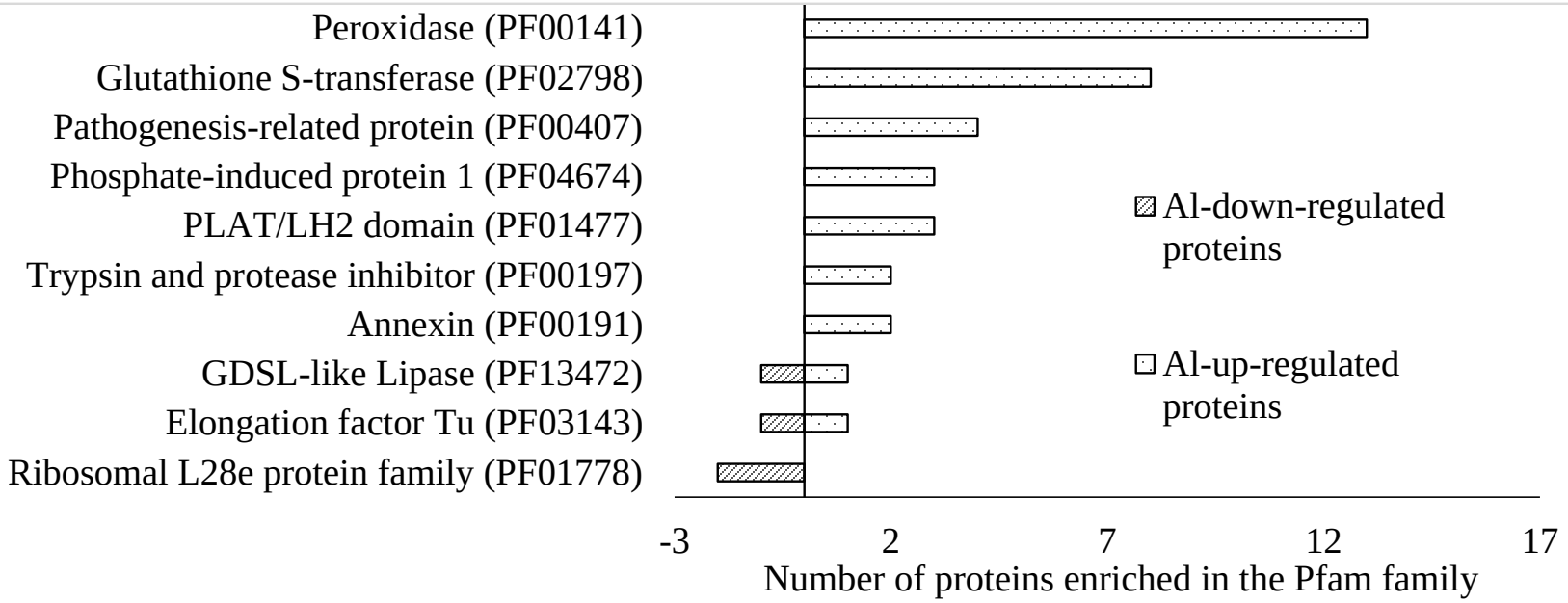

Fig.5. Pfam family of Al-induced differential expressed proteins in tomato root tips.

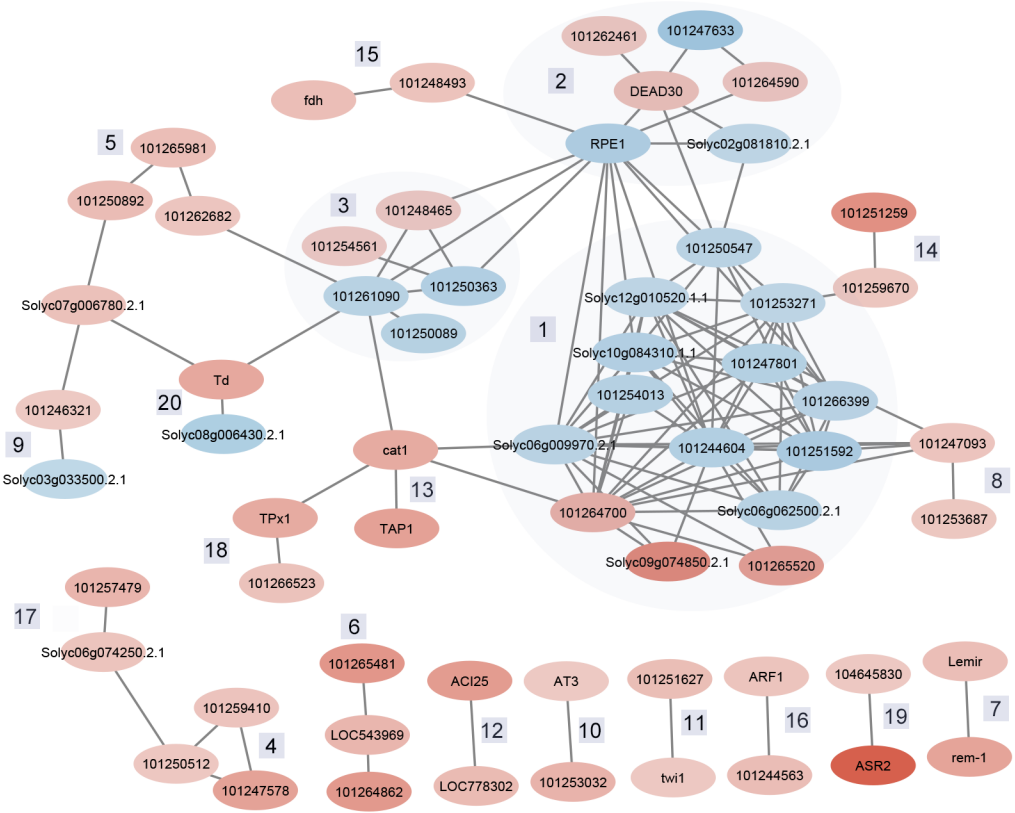
101262461
101247633
15
101248493
fdh
2
DEAD30
101264590
RPE1
Solyc02g081810.2.1
5
101265981
101250892
101262682
3
101248465
101254561
101261090
101250363
101250089
101251259
14
101259670
101250547
Solyc12g010520.1.1
101253271
Solyc07g006780.2.1
1
Solyc10g084310.1.1
101247801
Td
101254013
101266399
101246321
20
Solyc08g006430.2.1
9
Solyc03g033500.2.1
cat1
Solyc06g009970.2.1
101244604
101251592
101247093
8
13
TPx1
TAP1
101264700
Solyc06g062500.2.1
101253687
18
Solyc09g074850.2.1
101265520
101266523
101257479
17
Solyc06g074250.2.1
6
101265481
ACI25
AT3
101251627
ARF1
104645830
Lemir
101259410
LOC543969
12
10
11
16
19
7
4
101250512
LOC778302
101253032
twi1
101244563
ASR2
rem-1
101247578
101264862

Fig.6.

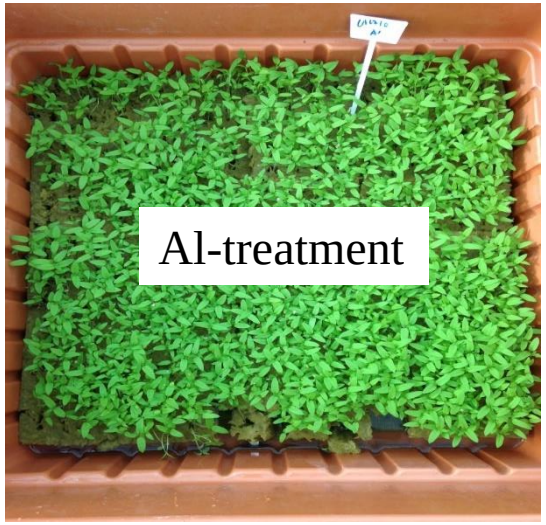

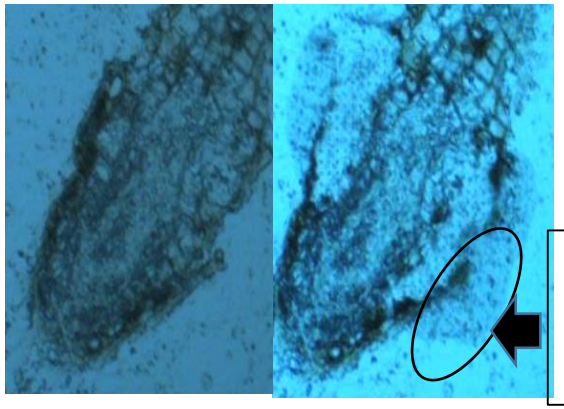

Tissue collection using Laser capture microdissection

Protein extraction

Purification

Trypsin Digestion

Labeling

Mass-spectrometry analysis

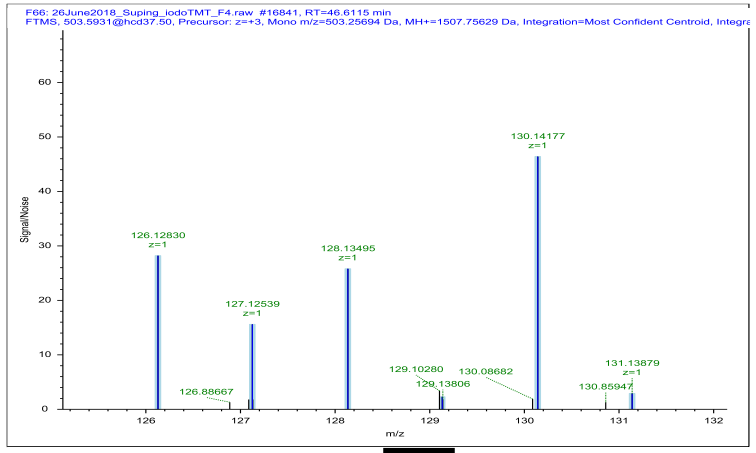

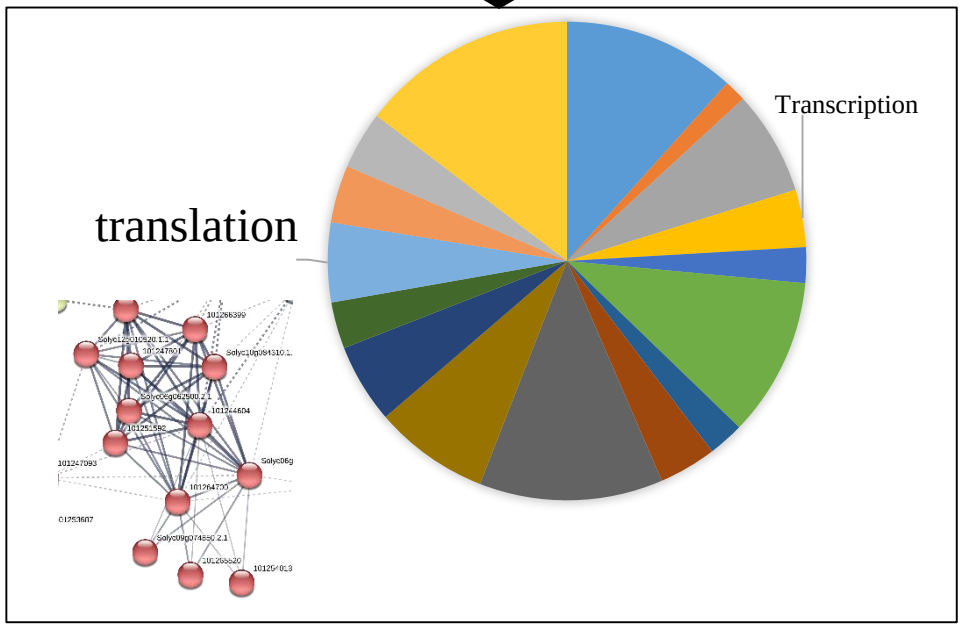

Graphic Abstract